Reduction of oxygen in a trialkoxy ammonium-based ionic liquid and the role of water

Reduction of oxygen in a trialkoxy ammonium-based ionic liquid and the role of water

Cristina Pozo-Gonzalo[a*], Mega Kar[b], Erlendur Jónsson[a], Patrick C. Howlett[a], Douglas R MacFarlane[b], Maria Forsyth[a]

[a]ARC Centre of Excellence for Electromaterials Science, Deakin University, 221 Burwood Hwy, Burwood, Victoria 3125, Australia.

[b]ARC Centre of Excellence for Electromaterials Science, Monash University, Clayton, Victoria 3800, Australia.

Corresponding author: Cristina Pozo-Gonzalo

E-mail address: cpg@deakin.edu.au

Abstract

The oxygen reduction reaction in a novel trialkoxy ammonium-based ionic liquid, N-ethyl-2-(2-methoxyethoxy)-N,N-bis(2-(2-methoxyethoxy)ethyl)ethan-1-aminium bis(trifluoromethylsulfonyl)imide, [$N_{2(20201)(20201)(20201)}$] [$NTf_2$] has been studied on glassy carbon and gold electrodes, showing faster electrokinetics on glass carbon because of weaker adsorption of the IL. This has been demonstrated by theoretical calculations and electrochemical studies. In the neat IL, the oxygen is reduced to superoxide ($O_2^{\bullet -}$) through a one electron process; however, better performance is attained in the presence of water (42 mol%), in terms of current density, and onset potential of the reduction process via a reversible 2-electron process. Furthermore, a remarkable increase in cyclic coulombic efficiency is observed for the wet IL (66 % in comparison with the neat IL (24 %), showing the practicality of a reversible O_2/H_2O_2 system for energy storage.

Keywords

Oxygen reduction, trialkoxy ammonium ionic liquid, superoxide, hydrogen peroxide, Au

Introduction

Metal-air batteries have received a great deal of attention due to their high theoretical energy densities, up to 5kWh kg^{-1} which is approximately 7−8 times that of today's best Li-ion batteries. [1] This promising technology could support advanced electronic equipment, as well as emerging applications, such as electric vehicles. A metal-air battery is composed of a metallic anode (e.g. lithium, zinc or magnesium) and an air cathode (deliberately open to the air to allow dioxygen inside the cell), which are separated by an electrolyte. One of the main reasons for the high energy density in these batteries is the use of oxygen as one of the active materials; oxygen is not stored within the battery, thus decreasing the weight of materials in the device. Importantly, because air is infinite and constantly available, metal-air batteries are expected to be a low cost technology.

However, the open to the atmosphere design causes conventional aqueous and non-aqueous electrolytes to dry out, leading to failure of the batteries. In this regard, ILs are a promising alternative electrolyte because they are non-volatile and generally highly chemically and electrochemically stable. Typical ILs are entirely composed of large asymmetric cations and small symmetric anions; the number of possible cation-anion combinations is very large, allowing tailoring of electrolyte properties to suit the final application. The use of ILs electrolytes in metal-air batteries has been explored and recently a comprehensive perspective on currents advances in IL electrolytes for Li, Na, Mg and Al air batteries has been published

[2]. The electrochemical stability of the IL is a key property that allows the plating and stripping of some of these metals (e.g. Na, Al, Zn) that is not possible in other media.

There remain a number of challenges to overcome when using ILs as electrolytes. For instance, the metal cations (M^{n+}) released during the discharge process of the metal-air battery can either be solvated by the electrolyte or, in the worst case scenario, form insoluble salts that clog the air cathode, significantly limiting the access of oxygen in the battery, [3] and deteriorating its performance, eventually to the point of failure. Thus, increasing the solvation of the metal cations, and therefore their solubility in the electrolyte, should enhance the performance of the battery, and also improve its energy efficiency by reducing the overpotentials.

For instance, the addition of the oligoether N,N-diethyl-N-methyl-N-(2-methoxyethyl)ammonium bis(trifluoromethylsulfonyl)imide, $[N_{1,2,2,102}][NTf_2]$, into an ethylmagnesiumbromide/tetrahydrofuran solution improved the Mg cycleability due to the solvation of metal cations by alkoxy chains [4]. More recently, Kar et al. [5, 6] synthesised innovative RTILs composed of an alkoxy ammonium cation and NTf_2 based-anion in order to stabilise Zinc metal cations.

Moverover, the oligoether chains are rather flexible, and usually lower the melting point, decrease the T_g and viscosity, and increase the conductivity of most quaternary ammonium-based ILs [7].

From the secondary battery point of view, metal plating and stripping reactions, along with oxygen reduction and evolution need to occur efficiently. In ILs, unlike aqueous media, the oxygen reduction generally involves the exchange of 1 electron in a reversible manner, generating superoxide ($O_2^{\bullet-}$) as the final product [8]. The reversibility of the O_2 /$O_2^{\bullet-}$ redox couple in aprotic ILs has been the focus of research for over more than 10 years [8]. Among

the different families of ILs, aliphatic tetraalkylammonium and alicyclic pyrrolidinium-based ILs have showed outstanding reversible O_2 /$O_2^{\bullet-}$ reaction pairs with ratio of anodic to cathodic current densities, (j_{pa}/j_{pc}) of 0.97 for [$N_{2,2,2,6}$][NTf_2] and 0.93 for [C_4mpyr][NTf_2] [9]. This reversibility is attributed to the ion pairing, and thus stabilization, between the superoxide and the organic ammonium ions [10]. However, limited coulombic efficiency has been described for some ILs resulting from; i) the nature of the IL, especially imidazolium-based ILs [11],[9],[12] which are susceptible to attack by the reactive superoxide anion at the carbon in the 2-position, [9] ii) differences in diffusion coefficient for the oxygen and superoxide anion caused by coulombic interactions, mostly between superoxide anion and the cation of the IL, and iii) subsequent reactions involving protonation and disproportionation steps [2],[13],[14].

Therefore, an IL capable of stabilising both the superoxide anion (produced by the reduction of oxygen) and the metal cations (produced during the discharge process) would be a substantial step forward for metal-air batteries. We hypothesize that an aliphatic quaternary ammonium cation with oligoether side chains should have those capabilities. Thus we examine here the oxygen reduction and evolution reactions in [$N_{2(20201)(20201)(20201)}$] [$NTf_2$], N-ethyl-2-(2-methoxyethoxy)-N,N-bis(2-(2-methoxyethoxy)ethyl)ethan-1-aminium bis(trifluoromethylsulfonyl)imide, under dry conditions and find the $O_2/O_2^{\bullet-}$ redox couple to be reversible on both glassy carbon (GC) and gold (Au) electrodes. However, the nature of the working electrode affected the performance, with GC showing higher current density and lower peak potential separation; these differences are explained by computational studies.

In addition, we report a highly reversible O_2/H_2O_2 redox couple (a 2-electron process) in wet [$N_{2(20201)(20201)(20201)}$] [$NTf_2$]. This system shows an impressive increase in both charge and coulombic efficiency when compared with the dry analogue (*ca.* cyclic coulombic efficiencies: 66.3 % and 23.6% for the wet and dry, respectively). Furthermore, no

degradation was observed over 20 cycles at different applied currents. Although a highly reversible one-electron process has been reported for a wide range of ILs, especially in the absence of water, highly reversible 2-electron processes have not be reported in ionic liquids. Thus we now show its suitability for reversible oxygen reduction and evolution through 1 (neat IL) or 2 (wet IL) electron pathways.

Experimental

The synthesis of the ionic liquid [$N_{2(20201)(20201)(20201)}$] [$NTf_2$], N-ethyl-2-(2-methoxyethoxy)-N,N-bis(2-(2-methoxyethoxy)ethyl)ethan-1-aminium bis(trifluoromethylsulfonyl)imide (Scheme 1), is described elsewhere. [15] The water content of 200 ppm in the ionic liquid was determined by Karl-Fischer titration (Metrohm KF 831 Karl Fischer Coulometer).

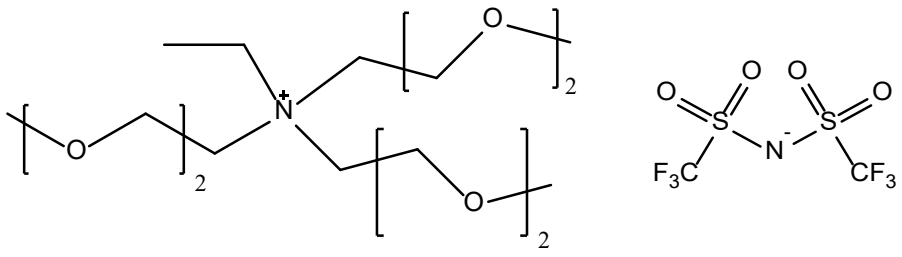

Scheme 1

Electrochemical experiments were performed with a Biologic VMP3/Z multi-channel potentiostat using a standard 3-electrode set-up, with a Pt wire counter electrode. A Ag/AgCl reference electrode was manufactured by immersing a Ag/AgCl wire into a capillary containing the IL separated from the bulk solution with a porous frit. Glassy carbon (GC, 1

mm diameter, ALS Co., Ltd. Japan) and Gold (Au, 1.6 mm diameter, ALS Co., Ltd. Japan) were used as the working electrode. Cyclic voltammetry was performed at 10 mV s^{-1} scan rate. The reference electrode was calibrated versus Fc/Fc^{+} (E_m: -0.23 V). All of the experiments were performed at 20 ± 1 °C.

Prior to any scan, the working electrode was polished with 0.3 μm alumina and then washed with deionised water (Millipore SuperQ system, resistivity 18.2 MΩ cm^{-1}). The measurements were carried out with an IR drop compensation prior to the cyclic voltammetry experiments, which compensated for approximately 85% of the total internal resistance. The ionic liquids were bubbled with oxygen (ultrahigh purity grade, Air Liquide) for 30 min prior to performing the voltammetry measurements, and bubbled again between scans. Control experiments were performed inside a glovebox in a nominally oxygen-and moisture-free environment.

The dynamic viscosities were determined using the rolling ball method at 25ºC, a capillary diameter of 2.5 mm and an angle of 60° (Anton Paar Lovis 2000ME), considering the density determined at the same temperature with the density meter Anton Paar DMA5000. The ionic conductivity of the samples was evaluated using AC impedance spectroscopy in a frequency range of 0.1 Hz to 10 MHz in a dip cell. The measurements were performed with a frequency response analyser, Solartron 1296, driven by Solartron impedance measurement software version 3.2.0.

Adsorption energies were calculated for four distinct systems (refer to Scheme 2 for cations); tetraethylammonium cation, $[N_{2,2,2,2}]^{+}$, tetraethylammonium cation superoxide ion pair, $[N_{2,2,2,2}][O_2]$, N-ethyl-2-methoxy-N,N-bis(2-methoxyethyl)ethan-1-aminium cation, $[N_{2(201)(201)(201)}]^{+}$ (a simplified version of the $[N_{2(20201)(20201)(20201)}]^{+}$ system), and N-ethyl-2-methoxy-N,N-bis(2-methoxyethyl)ethan-1-aminium cation superoxide ion pair $[N_{2(201)\ (201)}$

$_{(201)}$][O_2], for model surfaces of both GC and Au electrodes. In order to understand the role of oxygen in the alkyl chains, an alkyl chain analogue was also chosen. A few conformer variations were also considered.

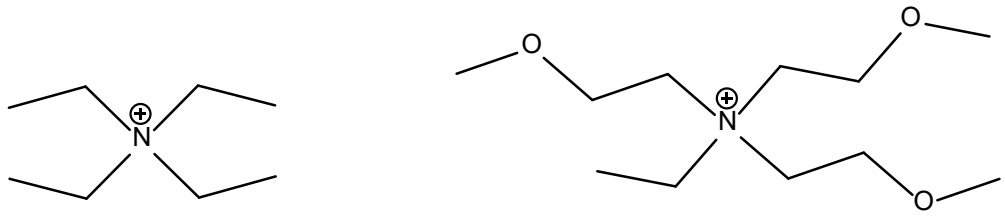

$[N_{2,2,2,2}]^+$ $[N_{2(201)(201)(201)}]^+$

Scheme 2

The model electrode systems were a graphene analogue, endcapped with hydrogen to ensure a singlet state ($C_{112}H_{30}$), and a Au(111) slab, chosen for its electrocatalytic properties, comprising 6x6x2 atoms with lattice constant a=4.080 Å. The cations and ion-pairs were then optimised (the electrodes were kept fixed). After convergence (energy defined as E_{sys}), separate single point calculations for the molecules (E_{mol}) and electrodes (E_{el}) were performed, giving adsorption energies:

$$\Delta E_{ads} = E_{sys} - E_{mol} + E_{el}$$

All calculations used the GPW scheme [16] with the dispersion corrected[17] PBE functional[18] with the TZVP MOLOPT basis set on all atoms except Au (which used DZP-

MOLOPT-SR) [19] and GTH pseudopotentials[20],[21],[22]. The MT Poisson solver [23] was used with a non-periodic box size of 22 Å on all axes. The orbital transform[24] method was used with the full kinetic preconditioner. For calculations with the superoxide the ROKS option was used. All calculations used CP2K version 2.6.0 [25].

RESULTS AND DISCUSSION

Electrochemical measurements

Figure 1a and b depict the electrochemical performance of the trialkoxy ammonium IL $[N_{2(20201)(20201)(20201)}]$ $[NTf_2]$ saturated with oxygen using glassy carbon and gold electrode, respectively, as working electrodes. Two cathodic processes, C1 and C2, and one oxidation process, A, are observed; the redox processes differ depending on the nature of the working electrode.

Fig. 1.

The potentials for the cathodic processes, C1 and C2 are slightly more negative for Au working electrodes than for GC (Table 1). In terms of current density, the peak current density of both cathodic processes, C1 and C2, seems independent of the nature of the working electrode, and peak currents up to 0.4 mA cm^{-2} were achieved.

However, the nature of the working electrode strongly affects the anodic process, A, showing a more efficient electrochemical cycling of oxygen on glassy carbon (e.g. peak current density for the anodic process of just 0.02 mA cm^{-2} on Au, and 0.09 mA cm^{-2} on GC).

Table 1.

Successive scans up to 10 cycles were performed to explore the nature of the redox processes C1, C2 and A using both GC (Figure 1c) and Au working electrodes (Figure S1). Upon cycling, the small reduction peak at *ca*. -1.3 V disappears for both working electrodes Furthermore, the cathodic process, C1 reappears with the same current density, (without polishing the surface of the working electrode) when restoring the oxygen concentration in the ionic liquid. This performance is more consistent with an adsorption process on the electrode than with a faradaic process.

Additionally, according to the literature where similar pre-waves have been reported, this process, C1, could be due to the reduction of the oxygen adsorbed on the surface of the electroactive material, as already reported for pyrrolidinium-based ILs [26].

Therefore, only the cathodic process C2 and the anodic process A are due to the bulk oxygen reduction (ORR) and oxygen evolution (OER). Those processes are consistent with previous research work on the ORR in the tetraalkyl ammonium ionic liquid $[N_{2226}][NTf_2]$, where they were ascribed to the O_2/ $O_2^{\bullet-}$ redox couple with similar onset reduction potential (*ca.* Au = -1.19 V vs Ag/Ag^+) [9].

In addition, an interesting increase in current density upon cycling for the anodic process for both working electrodes is depicted in Figure 1d.

At the tenth scan, the peak potential separation for GC is 0.11 V while in the case of Au this value is doubled (ca. 0.22 V), consistent with faster heterogeneous electron transfer kinetics in the case of GC (Figure 1d). This phenomenon is not only limited to tetraalkylammonium-

based ionic liquids, but has also been observed in imidazolium-based ionic liquids when comparing Pt, GC and Au, where the rate constant was found to increase in the order k^0 (Pt) < k^0 (Au) < k^0 (GC) [27].

Interestingly, several reports have focused on the electrode interfaces of Au and GC with tetraalkylammonium–based supporting electrolytes in acetonitrile in an oxygen-saturated environment.[10], [28] For instance, Aldous et al.[28] studied the effect of the length of alkyl chains in tetraalkylammonium cations on Au and GC surfaces. Unchanged performance for the O_2/ $O_2^{\bullet-}$ redox couple was observed for GC, which is consistent with negligible adsorption; however, on a gold surface inferior electrokinetic performance was observed with increasing alkyl chain length because of enhanced adsorption on the gold surface. Furthermore, Aldous et al. [28] explained that for a given alkyl chain length the adsorption is stronger on Au than on GC. When adsorption is dominant, partial blocking of the surface is expected to occur, which will limit the rates of oxygen reduction and evolution; this is consistent with our findings. Both Peng et al. [10] and Aldous et al. [28] have been able to observe and identify a film on the Au electrode surface using SERS (surface enhanced Raman spectroscopy); the nature of the film is consistent with the ion pairs involving tetraalkylammonium cations and superoxide anions.

Computational results

To better understand why the behaviour of the trialkoxy ammonium system depends on the nature of the working electrode, computations were designed that would be feasible for this system and would also give a comparison with an alternative cation. Although the chosen computations are not sufficient to fully reveal the details of the ORR, they should allow us to explain the qualitative differences. Thus, the adsorption energies of $[N_{2,2,2,2}]^+$ and $[N_{2(201)\,(201)}$

$_{(201)}]^+$ (Scheme 2), and the corresponding cation-superoxide ion pairs on graphene and gold were determined. While these computed systems are a very simplified version of the full system, $[N_{2(20201)(20201)(20201)}]$ $[NTf_2]$, they are illustrative, as they show that there is a substantial difference between how the $[N_{2,2,2,2}]^+$ and $[N_{2(201)\ (201)\ (201)}]^+$ cations interact with the superoxide anion.

There is some difference in how strongly the cations interact with the electrodes. However, the largest difference is how strongly the $[N_{2(201)(201)(201)}][O_2]$ ion-pair interacts with gold in comparison to with graphene. As Table 2 shows, the $[N_{2(201)(201)(201)}]^+$ clearly binds more strongly to gold than to graphene, with a $\Delta(\Delta E)$ (i.e. the difference in their corresponding ΔE_{ads}) of 2.85 eV, which is consistent with the inferior performance observed for Au in Figure 1d in terms of cathodic and anodic peak current as well as peak potential separation, when compared with GC.

A similar result was found for the $[N_{2,2,2,2}]^+$, with $\Delta(\Delta E)$ of 1.81 eV. The ion-pair calculations are also qualitatively similar; however, the energy differences are much larger, with $\Delta(\Delta E)$ values of 8.96 eV and 6.36 eV for the $[N_{2,2,2,2}]$ $[O_2]$, and $[N_{2(201)(201)(201)}]$ $[O_2]$, ion pairs, respectively.

Table 2

Comparing the adsorption energies of the cations and ion-pairs on graphene shows that, for both the $[N_{2,2,2,2}]^+$ and $[N_{2(201)(201)(201)}]^+$ there are only slight increases in adsorption energy for ion-pairs. The difference are 0.89 eV and 0.71 eV for $[N_{2,2,2,2}]^+$ and $[N_{2(201)(201)(201)}]^+$, respectively. For Au, these differences are increased substantially, to 5.44 eV and 6.82 eV for $[N_{2,2,2,2}]^+$ and $[N_{2(201)(201)(201)}]^+$, respectively.

Interestingly, looking at the final structures of the optimised ion-pairs, $[N_{2,2,2,2}][O_2]$ and $[N_{2(201)(201)(201)}][O_2]$, it is notable that the superoxide is always above the cation, i.e. not adsorbed directly on the electrode (Figure 2).

Fig. 2.

Effect of water on the electroreduction of oxygen

Due to the superior electrokinetics of the ORR on GC, the effect of water in $[N_{2(20201)(20201)(20201)}]$ $[NTf_2]$ on the ORR was only evaluated using GC. It is important to remember that air cathodes are open to the atmosphere, so water uptake by the electrolyte over time is expected; therefore understanding the role of water in the ORR mechanism is paramount.

Figure 3a shows the electrocatalytic properties of GC in the O_2-saturated trialkoxyammonium IL, $[N_{2(20201)(20201)(20201)}]$ $[NTf_2]$, upon the addition of 1.42 mmol H_2O/g IL (*ca.* 2.5%w/w or 42 mol %) to give "wet IL". Two reduction processes, C1 = -1.24 V and C2= -1.31 V, and one oxidation process, A = -0.84 V, were observed when scanning the potential between -0.4 and -1.6 V vs Ag/AgCl.

Fig. 3.

Upon cycling, process C1 disappears progressively without cleaning the working electrode, as was also seen for the neat IL (*cf*. Figure 3b).

The onset for cathodic process C2 in the wet IL is 0.21V more positive than it was in the neat IL (Figure 3c). It is known that a shift in the $E^{0'}$ value for a redox couple can be caused by the polarity of the solvent, nature of the electrolyte or the presence of acidic additives owing to nonspecific solvation energies, ion pairing and proton activity/protonation equilibria, respectively [29],[12],[30]. The effect of water in the ORR mechanism in ionic liquids has been studied in phosphonium-based ILs [31], as well as in imidazolium-based ILs [9]. In general, an increase in current density is observed because of more favourable mass transport conditions, as well as a shift of the reduction potential to more positive values owing to changes in the proton activity, and therefore on the protonation equilibria and solvation of the electrogenerated species ($O_2^{\bullet-}$, O_2^{2-}) [8].

Similar features (i.e. increased current density and positive shift of the reduction process onset) are observed here with for the $[N_{2(20201)(20201)(20201)}]$ $[NTf_2]$ upon addition of water. The physicochemical properties of the IL upon water addition are clearly superior (Table 3). For instance, the viscosity is reduced from 99.6 to 48. 9 mPa s and the conductivity increased from 0.0011 to 0.0015 S cm^{-1} upon water addition.

Table 3.

More importantly, the increase from one- to two-electron transfer could be the most likely cause of the increased peak currents. The presence of water in the IL appears to modify the oxygen reduction mechanism from one electron, leading to superoxide ($O_2^{\bullet-}$), to a 2-electron pathway which generates H_2O_2 (or HO_2^-) as the final product. For instance, 1-ethyl-3-methylimidazolium tetrafluoroborate, $[C_2mim][BF_4]$, containing 2.64 M water (*ca*. 2.6 mmol H_2O/g IL) was shown by Zhang et al to lead to an increase in electron transfer from a reversible one-electron process to an irreversible 2-electrons process [27]. However, smaller

concentrations of water (e.g. 0.5 vol% corresponding to approximately 0.28 mmol H_2O/g IL) in 1-ethyl-3-methylimidazolium bis(trifluoromethanesulfonyl)imide,[C_2mim][NTf_2] [9] produced an increase in electron transfer and also an anodic process in the reverse scan in a similar manner as that seen in the present case (Figure 3a)], and leading to one of the first examples of reversible O_2 / H_2O_2 couple.

Additionally, the superoxide ion has been generated in a stable manner in the trihexyl(tetradecyl)phosphonium chloride IL, [$P_{6,6,6,14}$][Cl], in the presence of large quantities of water (*ca.* 2.5 mmol H_2O/g IL) because of strong ion pairing between the superoxide ion and the phosphonium cation [32]·[33].

The protonation mechanism of superoxide in the presence of weak acids has been studied in ionic liquids by René et al. [14], corresponding to successive chemical and electrochemical reactions denoted as ECE-DISP mechanism:

$$O_2 + 1e^- \rightleftharpoons O_2^{\bullet -} \quad (1)$$

$$O_2^{\bullet -} + H_2O \rightleftharpoons HO_2^{\bullet} + HO^- \quad (2)$$

$$HO_2^{\bullet} + O_2^{\bullet -} \rightleftharpoons O_2 + HO_2^- \quad (3)$$

$$HO_2^- + H_2O \longrightarrow H_2O_2 + HO^- \quad (4)$$

The ORR mechanism begins with the 1-electron reduction process O_2 / $O_2^{\bullet -}$ (1) followed by protonation of the superoxide anion by water, as the proton source, to generate $HO_2^{\bullet}$ (2) which is immediately reduced in solution by another $O_2^{\bullet -}$ yielding HO_2^- and O_2 (3). $HO_2^{\bullet}$ can undergo various reactions mechanism depending on the nature of the electrolyte and on the activity of the proton source. A compressive chapter on the mechanisms of $HO_2^{\bullet}$, and ORR in non-aqueous media, has been recently published by Pozo-Gonzalo [8].

The final step of the mechanism (4) involves the protonation of HO_2^-. Thus, the overall 2 electron reaction is reported in equation (5).

$$2O_2 + 2H_2O + 2e^- \rightleftharpoons H_2O_2 + 2\,HO^- \quad (5)$$

Consecutive scans were applied to the O_2-saturated wet IL (Fig. 3b) leading to an outstanding enhancement in anodic peak current A, from 0.19 in the first scan to 0.47 mA cm^{-2} in the 10^{th} scan, while the peak current density for the reduction of oxygen remained constant. This increase of the anodic current density could be related to an activation of the surface during cycling which may lead to different active surface area.

The cycleability of the O_2/H_2O_2 process has barely been previously explored in the literature. Thus, a more detailed study of the cycleability of this redox couple is described below.

Oxidation/Reduction cyclability

A great deal of attention has been given to the reversibility of the O_2 /$O_2^{\bullet-}$ redox couple, however the reversibility for the O_2 /O_2^{2-} (or HO_2^-, H_2O_2) redox couple has been neglected because of lack or limited reversibility under the conditions used in previous studies.

In this work, we have examined the cycleability of the oxygen reduction and evolution using a GC working electrode. Chronopotentiometry results for the neat IL and the wet IL are shown in Fig. **4**. In both cases the potential was limited to avoid degradation of the IL and irreversible side reactions involving the oxygen electrogenerated species (i.e. to between -1.7 V and -1.2V for the neat IL and -1.5 and -0.4 V for the wet IL).

Fig. 4.

Significant differences are observed in the chronopotentiograms depending on the nature of the IL. For instance, at low current for the neat IL (i.e. ± 0.2 mA cm^{-2}) (Fig. 4a) during the anodic cycle, the depletion of the superoxide occurs around -1.3 V which is consistent with oxygen reduction and evolution depicted in the cyclic voltammogram in Fig. 1d. This behaviour appears unchanged for 20 cycles suggesting the stability of the reversible O_2 /$O_2^{\bullet-}$ process under those conditions.

For the wet IL, during the oxidation process, depletion of the reacting species is observed around -0.75 V. The mixture was also cycled for 20 cycles showing stable charge capacity and efficiency between cycles and demonstrating its viability as a rechargeable O_2/H_2O_2 system (Fig. 4 c and d).

In both electrolytes, the current was increased to ± 0.4 and ± 0.6 mA cm^{-2}, yielding profiles similar to those seen at low current. The charge for the oxidation and reduction processes was calculated at each current for the neat and wet IL (*cf.* Table 4), showing lower values at high current values. This behaviour is expected because of the potential cut-off limit in the charge/discharge process. This, in turn, significantly reduces the time allow for the oxidation and reduction processes to take place when increasing the applied current.

However, the cyclic coulombic efficiency is considerably enhanced at higher current values which can be explained by limited time for the electrogenerated species react in the bulk electrolyte or diffuse away. Further studies to clarify the nature of such enhancement will be the goal of future work.

At a particular current *ca*. ± 0.2 mA cm^{-2}, the wet IL shows superior performance, in terms of charge and coulombic efficiency (e.g. coulombic efficiency: 24 versus 66 % for the neat IL and wet IL, respectively).

Table 4.

Conclusions

In $[N_{2(20201)(20201)(20201)}]$ $[NTf_2]$ under dry conditions the oxygen reduction and evolution reactions are a reversible O_2 /$O_2^{\bullet-}$ redox couple on both GC and Au electrodes. The GC electrodes gave superior performance, in terms of current density and peak potential separation. This was attributed to the stronger adsorption of the IL cation and ion pair with superoxide on Au, as demonstrated by theoretical calculations; this strong adsorption explains the inferior electrokinetics of oxygen reduction and evolution on Au in comparison to on GC.

The role of water in the ionic liquid has been investigated leading to improved performance in terms of onset for the reduction process as well as anodic and cathodic peak current. The wet IL shows substantial improvements in mass transport, and cathodic and anodic coulombic efficiencies as well as a reversible 2-electron process.

Acknowledgments

The authors gratefully acknowledge the financial support from the Australian Research Council (ARC) through the ARC Centre of Excellence for Electromaterials Science (ACES). MF and DRM also gratefully acknowledge funding through the ARC Laureate program.

References

[1] C.J. Allen, J. Hwang, R. Kautz, S. Mukerjee, E.J. Plichta, M.A. Hendrickson, K.M. Abraham, Oxygen Reduction Reactions in Ionic Liquids and the Formulation of a General ORR Mechanism for Li–Air Batteries, The Journal of Physical Chemistry C, 116 (2012) 20755-20764.

[2] M. Kar, T.J. Simons, M. Forsyth, D.R. MacFarlane, Ionic liquid electrolytes as a platform for rechargeable metal-air batteries: a perspective, Phys Chem Chem Phys, 16 (2014) 18658-18674.

[3] F. Cheng, J. Chen, Metal-air batteries: from oxygen reduction electrochemistry to cathode catalysts, Chemical Society Reviews, 41 (2012) 2172-2192.

[4] N. Yoshimoto, M. Matsumoto, M. Egashia, M. Morita, Mixed electrolyte consisting of ethylmagnesiumbromide with ionic liquid for rechargeable magnesium electrode, Journal of Power Sources, 195 (2010) 2096-2098.

[5] M. Kar, B. Winther-Jensen, M. Forsyth, D.R. MacFarlane, Chelating ionic liquids for reversible zinc electrochemistry, Phys Chem Chem Phys, 15 (2013) 7191-7197.

[6] M. Kar, B. Winther-Jensen, M. Armand, T.J. Simons, O. Winther-Jensen, M. Forsyth, D.R. MacFarlane, Stable zinc cycling in novel alkoxy-ammonium based ionic liquid electrolytes, Electrochimica Acta, 188 (2016) 461-471.

[7] J. Reiter, E. Paillard, L. Grande, M. Winter, S. Passerini, Physicochemical properties of N-methoxyethyl-N-methylpyrrolidinum ionic liquids with perfluorinated anions, Electrochimica Acta, 91 (2013) 101-107.

[8] C. Pozo-Gonzalo, Oxygen reduction reaction in ionic liquids: An overview, Electrochemistry in ionic liquids, Springer2015.

[9] Y. Katayama, H. Onodera, M. Yamagata, T. Miura, Electrochemical reduction of oxygen in some hydrophobic room-temperature molten salt systems, J. Electrochem. Soc., 151 (2004) A59-A63.

[10] Z. Peng, S.A. Freunberger, L.J. Hardwick, Y. Chen, V. Giordani, F. Bardé, P. Novák, D. Graham, J.-M. Tarascon, P.G. Bruce, Oxygen Reactions in a Non-Aqueous Li+ Electrolyte, Angewandte Chemie International Edition, 50 (2011) 6351-6355.

[11] M.T. Carter, C.L. Hussey, Electrochemical Reduction of Dioxygen in Room-temperature Imidazolium Chloride-Aluminium Chloride Molten Salts, Inorganic Chemistry, 30 (1991) 1149-1151.

[12] M.M. Islam, T. Ohsaka, Roles of ion pairing on electroreduction of dioxygen in imidazolium-cation-based room-temperature ionic liquid, J. Phys. Chem. C, 112 (2008) 1269-1275.

[13] A.S. Barnes, E.I. Rogers, I. Streeter, L. Aldous, C. Hardacre, G.G. Wildgoose, R.G. Compton, Unusual voltammetry of the reduction of O-2 in C(4)dmim N(Tf)(2) reveals a strong interaction of O-2(center dot-) with the C(4)dmim (+) cation, Journal of Physical Chemistry C, 112 (2008) 13709-13715.

[14] A. Rene, D. Hauchard, C. Lagrost, P. Hapiot, Superoxide Protonation by Weak Acids in Imidazolium Based Ionic Liquids, Journal of Physical Chemistry B, 113 (2009) 2826-2831.

[15] M. Kar, B. Winther-Jensen, M. Forsyth, D.R. MacFarlane, M. Armand, Novel alkoxy-ammonium based room temperature ionic liquids for rechargeable zinc batteries and the effect of zinc ions and water on their physical properties, 2015.

[16] G. Lippert, M. Parrinello, A hybrid Gaussian and plane wave density functional scheme, Molecular Physics, 92 (1997) 477-488.

[17] S. Grimme, J. Antony, S. Ehrlich, H. Krieg, A consistent and accurate ab initio parametrization of density functional dispersion correction (DFT-D) for the 94 elements H-Pu, The Journal of Chemical Physics, 132 (2010) 154104.

[18] J.P. Perdew, K. Burke, M. Ernzerhof, Generalized Gradient Approximation Made Simple, Physical Review Letters, 77 (1996) 3865-3868.

[19] J. VandeVondele, J. Hutter, Gaussian basis sets for accurate calculations on molecular systems in gas and condensed phases, The Journal of Chemical Physics, 127 (2007) 114105.

[20] S. Goedecker, M. Teter, J. Hutter, Separable dual-space Gaussian pseudopotentials, Physical Review B, 54 (1996) 1703-1710.
[21] C. Hartwigsen, S. Goedecker, J. Hutter, Relativistic separable dual-space Gaussian pseudopotentials from H to Rn, Physical Review B, 58 (1998) 3641-3662.
[22] M. Krack, Pseudopotentials for H to Kr optimized for gradient-corrected exchange-correlation functionals, Theoretical Chemistry Accounts, 114 (2005) 145-152.
[23] G.J. Martyna, M.E. Tuckerman, A reciprocal space based method for treating long range interactions in ab initio and force-field-based calculations in clusters, The Journal of Chemical Physics, 110 (1999) 2810-2821.
[24] J. VandeVondele, J. Hutter, An efficient orbital transformation method for electronic structure calculations, The Journal of Chemical Physics, 118 (2003) 4365.
[25] J. VandeVondele, M. Krack, F. Mohamed, M. Parrinello, T. Chassaing, J. Hutter, Quickstep: Fast and accurate density functional calculations using a mixed Gaussian and plane waves approach, Computer Physics Communications, 167 (2005) 103-128.
[26] S. Monaco, A.M. Arangio, F. Soavi, M. Mastragostino, E. Paillard, S. Passerini, An electrochemical study of oxygen reduction in pyrrolidinium-based ionic liquids for lithium/oxygen batteries, Electrochimica Acta, 83 (2012) 94-104.
[27] D. Zhang, T. Okajima, F. Matsumoto, T. Ohsaka, Electroreduction of dioxygen in 1-n-alkyl-3-methylimidazolium tetrafluoroborate room-temperature ionic liquids, J. Electrochem. Soc., 151 (2004) D31-D37.
[28] I.M. Aldous, L.J. Hardwick, Influence of Tetraalkylammonium Cation Chain Length on Gold and Glassy Carbon Electrode Interfaces for Alkali Metal–Oxygen Batteries, The Journal of Physical Chemistry Letters, 5 (2014) 3924-3930.
[29] N. Gupta, H. Linschitz, Hydrogen-Bonding and Protonation Effects in Electrochemistry of Quinones in Aprotic Solvents, J Am Chem Soc, 119 (1997) 6384-6391.
[30] C. Pozo-Gonzalo, A.A.J. Torriero, M. Forsyth, D.R. MacFarlane, P.C. Howlett, Redox Chemistry of the Superoxide Ion in a Phosphonium-Based Ionic Liquid in the Presence of Water, J. Phys. Chem. Lett., 4 (2013) 1834-1837.
[31] C. Pozo-Gonzalo, C. Virgilio, Y. Yan, P.C. Howlett, N. Byrne, D.R. MacFarlane, M. Forsyth, Enhanced performance of phosphonium based ionic liquids towards 4 electrons oxygen reduction reaction upon addition of a weak proton source, Electrochemistry Communications, 38 (2014) 24-27.
[32] C. Pozo-Gonzalo, A.A.J. Torriero, M. Forsyth, D.R. MacFarlane, P.C. Howlett, Redox Chemistry of the Superoxide Ion in a Phosphonium-Based Ionic Liquid in the Presence of Water, The Journal of Physical Chemistry Letters, (2013) 1834-1837.
[33] C. Pozo-Gonzalo, P.C. Howlett, J.L. Hodgson, L.A. Madsen, D.R. MacFarlane, M. Forsyth, Insights into the reversible oxygen reduction reaction in a series of phosphonium-based ionic liquids, Phys Chem Chem Phys, 16 (2014) 25062-25070.